Calibration of the Flory-Huggins Interaction Parameter in Field-Theoretic Simulations

T. M. Beardsley and M. W. Matsen*

Department of Chemical Engineering, Department of Physics, and the Waterloo Institute for Nanotechnology, University of Waterloo, Waterloo, Ontario, Canada

(Dated: April 5, 2019)

Abstract

Field-theoretic simulations (FTS) offer a versatile method of dealing with complicated block copolymer systems, but unfortunately they struggle to cope with the level of fluctuations typical of experiments. Although the main obstacle, an ultraviolet (UV) divergence, can be removed by renormalizing the Flory-Huggins χ parameter, this only works for unrealistically large invariant polymerization indexes, $\bar{N}$. Here, we circumvent the problem by applying the Morse calibration, where a nonlinear relationship between the bare χ_b used in FTS and the effective χ corresponding to the standard Gaussian-chain model (GCM) is obtained by matching the disordered-state structure function, $S(k)$, of symmetric diblock copolymers to renormalized one-loop (ROL) predictions. This calibration brings the order-disorder transition (ODT) obtained from FTS into agreement with the universal results of particle-based simulations for values of $\bar{N}$ characteristic of experiment. In the limit of weak interactions, the calibration reduces to a linear approximation, $\chi \approx z_\infty \chi_b$, consistent with the previous renormalization of χ for large $\bar{N}$.

This manuscript was accepted by J. Chem. Phys. Click here to see the version of record.

I. INTRODUCTION

The standard Gaussian-chain model (GCM)[1] underpins most calculations for block copolymer melts, including the self-consistent field theory (SCFT) of Helfand,[2] the random-phase approximation (RPA) of Leibler[3], the strong-stretching theory (SST) of Semenov,[4] and the fluctuation theory of Fredrickson and Helfand.[5] The GCM treats block copolymer melts as an incompressible system of thin elastic threads interacting by simple contact forces. It is a minimal model that contains only the essential features of the system, and as such involves the least number of parameters possible. In the mean-field approximation, the equilibrium behavior of monodisperse AB diblock copolymers is controlled by just three quantities: the composition of the diblock, f, the ratio of segment lengths, a_A/a_B, and the product, χN, where χ is the Flory-Huggins interaction parameter and N is the total number of segments.[6] Fluctuation corrections to the mean-field behavior are then controlled by one additional parameter, the invariant polymerization index $\bar{N} = a^6\rho_0^2 N$, where $a = [fa_A^2 + (1-f)a_B^2]^{1/2}$ is the average segment length and ρ_0 is the segment density.[5] Note that we follow the standard practice of defining all segments to have a common volume of ρ_0^{-1}.

It is believed that all models as well as experimental systems reduce to the standard GCM at large N.[7] How large N needs to be will depend on the particular system. The universality implies that the parameters of any particle-based model can be mapped onto those of the GCM. The mapping of molecular compositions (e.g., f) is trivial given their straightforward definition in terms of volume fraction. The segment lengths are also clearly defined by the requirement that the average end-to-end length or radius of gyration of a linear homopolymer in a neat melt reduces to $R_0 = aN^{1/2}$ or $R_g = a(N/6)^{1/2}$, respectively, for large N.

The only nontrivial part of the mapping is the relationship between the χ parameter of the GCM and some corresponding parameter of the particle-based model, α, specifying the strength of its A-B interactions in units of k_BT. One important constraint is that the behavior of the particle-based model must approach SCFT in the $N \to \infty$ limit. Müller and Binder[8] proposed a linear relationship, $\chi = z(N)\alpha$, that satisfies this requirement, where $z(N)$ measures the number of intermolecular contacts between molecules of polymerization N in the athermal limit (i.e., $\alpha = 0$). This, however, results in a χ parameter that not only depends on molecular weight but also on molecular architecture. Such dependences would

sincerely limit the predictive power of block copolymer theory. Working on the assumption that such dependences are not necessary, Morse and coworkers[9] proposed that χ be defined as a nonlinear function of α, which reduces to $\chi \approx z_\infty \alpha$ for small α, where $z_\infty \equiv \lim_{N\to\infty} z(N)$. The nonlinear dependence is determined by matching the behavior of the particle-based model to some prediction of the GCM. It could, in principle, be any quantity for any block copolymer system, but it is best to choose the most accurate prediction possible that permits fits to relatively large values of α. Therefore, Morse and coworkers[10] chose the renormalized one-loop (ROL) prediction for the disordered-state structure function, $S(k)$, of symmetric diblock copolymer melts.[11,12] The success of this calibration method has been remarkable, at least, for diblock copolymer melts.[13–16]

Given the universality of block copolymer behavior, it is possible to obtain quantitative predictions using very simple particle-based models.[15] However, even with simple models, it can be challenging to simulate blends and, in particular, complicated polymeric architectures. Field-theoretic simulations (FTS)[17,18,20] offer a way around this problem.[21–23] They simulate a field-based version of the standard GCM, obtained by applying the same transformations used in SCFT.[24] For systems involving two chemical species, the interaction energy is represented by the Hubbard-Stratonovich identity involving a composition field, $W_-(\mathbf{r})$, and the delta function enforcing incompressibility is replaced by a Fourier representation involving a pressure field, $W_+(\mathbf{r})$. This allows the polymer coordinates to be integrated out, leaving a mathematically equivalent Hamiltonian, $H[W_-, W_+]$, that depends only on the two fields. Rather than solving the statistical mechanics of the field-based model using the saddle-point approximation of SCFT, one simply performs a simulation.

FTS of diblock copolymer melts are particularly efficient at large $\bar{N}$, but they run into problems for the experimentally relevant conditions of $10^2 \lesssim \bar{N} \lesssim 10^4$. For instance, complex-Langevin simulations (CL-FTS) encounter an instability associated with the incompressibility condition.[25] Monte-Carlo simulations (MC-FTS) avoid it by applying the saddle-point approximation for $W_+(\mathbf{r})$, but their results still diverge when the spacing, Δ, of the grid used to represent the fields is reduced towards zero. Fortunately, this ultraviolet (UV) divergence has the simple effect of disordering the melt, which can be compensated for by expressing results in terms of a renormalized interaction parameter,[26]

$$\chi = \left(1 - \frac{6\alpha}{\pi^2} l\Lambda\right) \chi_b \ , \tag{1}$$

This manuscript was accepted by J. Chem. Phys. Click here to see the version of record.

where $\alpha = 1.2214$ for cubic grids,[27] $l \equiv 1/\rho_0 a^2$ is the packing length, $\Lambda \equiv \pi/\Delta$ is the wavevector cutoff, and χ_b is the bare interaction parameter used in the MC-FTS. Although this renormalization works well for large $\bar{N}$,[27] it fails just prior to the experimentally relevant regime. Vorselaars and Matsen[28] appeared to resolve the problem by modifying the renormalization of χ. The modification removed the divergence for diblock copolymers of $\bar{N} = 10^3$, but it later failed for binary homopolymer blends at values of $\bar{N}$ where the renormalization in Eq. (1) worked just fine.[29,30]

Here, we take a different approach. Rather than trying to remove the divergence, we fix Δ at a small finite value and apply the Morse calibration. The first step is the evaluation of z_∞, the relative number of intermolecular contacts in a neat melt of infinitely long homopolymers. Next, we define an effective

$$\chi = \frac{z_\infty \chi_b + c_1 \chi_b^2}{1 + c_2 \chi_b} , \tag{2}$$

where the fitting parameters, c_1 and c_2, are determined by matching the peak of $S(k)$ for symmetric diblock copolymers to ROL theory. To assess the calibration, we compare the order-disorder transition (ODT) for diblock copolymers of $\bar{N} \lesssim 10^4$ to

$$(\chi N)_{\mathrm{ODT}} = 10.495 + 41.0\bar{N}^{-1/3} + 123.0\bar{N}^{-0.56} . \tag{3}$$

The first two terms are the standard Fredrickson-Helfand (F-H) approximation,[5] and the third term is an empirical correction obtained from particle-based simulations.[13]

II. FIELD-THEORETIC SIMULATIONS

The field-theoretic model for systems with two chemically-distinct segments, A and B, involves a composition field, $W_-(\mathbf{r})$, that couples to the difference between the A and B concentrations and a pressure field, $W_+(\mathbf{r})$, that enforces a uniform segment density of ρ_0. For a diblock copolymer melt of n molecules, the field-based Hamiltonian is given by[18,20]

$$\frac{H[W_-, W_+]}{k_B T} = -n \ln Q + \rho_0 \int \left(\frac{W_-^2(\mathbf{r})}{\chi_b} - W_+(\mathbf{r}) \right) d\mathbf{r} , \tag{4}$$

where Q is the partition function for a single molecule subject to the two fields. It is given by

$$Q[W_-, W_+] = \int q(\mathbf{r}, N) d\mathbf{r} , \tag{5}$$

where $q(\mathbf{r},t)$ is a partial partition function for the first t segments of the molecule with the t'th segment constrained at position $\mathbf{r}$. This function satisfies a diffusion equation,

$$\frac{\partial q}{\partial t} = \frac{a^2}{6}\nabla^2 q - (W_+ \pm W_-)q \ , \tag{6}$$

with the initial condition $q(\mathbf{r},0)$=1. The '+' and '−' signs are used when the t'th segment is of type A and B, respectively. Equation (6) is solved numerically using a pseudo-spectral algorithm with Richardson extrapolation[31,32] and a step size of $\Delta t = 1$ (i.e., N corresponds to the number of integration steps along the polymer chain). We will later require an analogous partial partition function, $q^\dagger(\mathbf{r},t)$, for the last $N-t$ segments. It is obtained by integrating Eq. (6) with one side multiplied by -1 backwards in t, starting from $q^\dagger(\mathbf{r},N)=1$.

FTS are complicated by the fact that $W_+(\mathbf{r})$ is an imaginary-valued function, which in turn makes $H[W_-,W_+]$ a complex-valued quantity. As a result, the Boltzmann weight, $\exp(-H/k_BT)$, is no longer positive definite, and therefore standard simulation methods are not applicable. Fredrickson and coworkers[17–20] have dealt with this by performing complex Langevin simulations (CL-FTS). Alternatively, this complication can be avoided by replacing $W_+(\mathbf{r})$ with its saddle-point, $w_+(\mathbf{r})$, which approximates the incompressibility condition by $\phi_+(\mathbf{r})=1$, where

$$\phi_+(\mathbf{r}) = \frac{V}{NQ}\int_0^N q(\mathbf{r},t)q^\dagger(\mathbf{r},t)dt \tag{7}$$

is the mean-field approximation for the total concentration. The integral over t is evaluated using the Simpson quadrature and the saddle-point is located with Anderson-mixing iterations, as described in Ref. 32. It turns out that $w_+(\mathbf{r})$ is a real-valued function, which then allows for the usual methods of statistical mechanics such as ordinary Langevin simulations (L-FTS)[33,34] or Monte Carlo simulations (MC-FTS).[35,36]

Here, we perform MC-FTS for melts of $n=\rho_0 V/N$ diblock copolymers in cubic simulation boxes of volume $V=L^3$ with periodic boundary conditions. The fields are represented on a discrete grid with m points in each direction separated by a uniform spacing of Δ (i.e., $L=m\Delta$). The grid resolution is set to $\Delta=a$ and the segment density is set to $\rho_0=8/a^3$. Each Monte Carlo step (MCS) involves making a small change to $W_-(\mathbf{r})$, followed by the reevaluation of $w_+(\mathbf{r})$. The moves are accepted or rejected based on the standard Metropolis criterion. We alternate between two kinds of moves:[27] one in real space where $W_-(\mathbf{r})$ is changed at each grid point by amounts selected from a uniform distribution, and another in Fourier space where $W_-(\mathbf{k})$ is changed at each wavevector with a probability proportional to

ing RPA structure function, $S_{\mathrm{RPA}}(\mathbf{k})$, for $\chi N = 10$. The amplitude of each move is adjusted during the beginning of the equilibration period to achieve an acceptance rate of $\sim 40\%$. We typically use 10^6 MCS to equilibrate the system, followed by $10^6 - 10^7$ MCS for the collection of statistics. Observables are generally sampled once every 10 MCS.

III. MORSE CALIBRATION

The first step of the calibration is to determine $z_\infty = \lim_{N\to\infty} z(N)$, the fraction of intermolecular contacts in a pure homopolymer melt of infinitely long chains. In particle-based simulations, it is necessary to evaluate $z(N)$ for finite polymers and then extrapolate to infinity, but here we are able to calculate z_∞ directly because of the saddle-point approximation and the absence of fields. The fact that $W_-(\mathbf{r})$ vanishes in the $\chi_b \to 0$ limit is obvious from the form of Eq. (4) or alternatively from the fact that the composition field cannot play any role in the absence of A-B interactions. Given that $W_-(\mathbf{r}) = 0$, it immediately follows that $\phi_+(\mathbf{r}) = 1$ is satisfied by $w_+(\mathbf{r}) = 0$.

Therefore, it suffices to consider a single infinite non-interacting chain, with its contour parameterized by $s = -\infty$ to ∞ and the $s = 0$ monomer constrained at the origin. It is important to remember that each coarse-grained segment of the GCM consists of an arbitrarily large number of monomers strung together; we are just constraining one monomer of negligible volume and not an entire segment. The segments will generally span multiple grid points, and hence the total number of segments at the origin, $\Delta^3\rho_0$, is not necessarily an integer. In any case, all we need to know is what fraction of the $\Delta^3\rho_0$ segments belong to the same chain as the constrained monomer, and thus experience an intramolecular contact with that monomer.

The calculation requires a propagator for the constrained chain providing the probability that the $s = t$ monomer is located at $\mathbf{r}$.[37] This propagator, $q_0(\mathbf{r}, t)$, satisfies the diffusion equation, with the initial condition $q_0(0, 0) = 1$ for the one grid point at the origin and zero for all other grid points. It is essential that $q_0(\mathbf{r}, t)$ be solved with the same numerical algorithm used in the FTS. The resulting quantity $q_0(0, t)$, plotted in Fig. 1, then provides the probability that the $s = t$ monomer is also at the origin. Thus, the integral of $q_0(0, t)$ gives the amount of chain, measured in segments, experiencing intramolecular contact with the constrained monomer. Due to the symmetry, it is sufficient to just integrate over positive

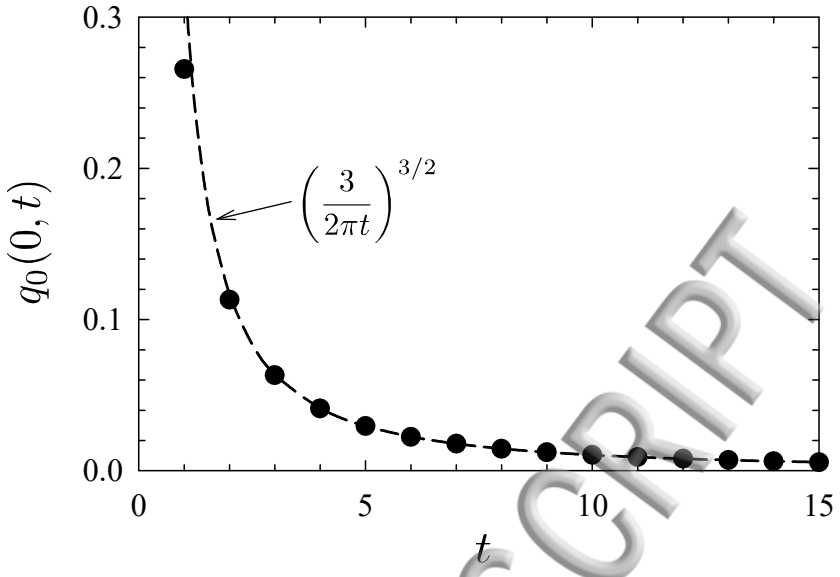

FIG. 1: Probability that a segment interacts with another segment t steps further along the same polymer chain, calculated for an athermal melt (i.e., $\chi_b = 0$). The dashed curve denotes an analytical approximation for large t.

t and then double the result. From that, we immediately obtain the fraction of intermolecular contacts,

$$z_\infty = 1 - \frac{2}{\Delta^3 \rho_0} \int_0^\infty q_0(0,t) dt = 0.7084 \ . \tag{8}$$

The numerical solution of $q(\mathrm{r},t)$, used to evaluate the Hamiltonian, is a discrete function of t, and so the integral in Eq. (8) should be evaluated accordingly. The issue is how the Q in Eq. (5) samples the fields, when χ_b is infinitesimally small. The Richardson extrapolation basically combines numerical solutions for full steps, $\Delta t = 1$, and half steps, $\Delta t = 1/2$, weighted by $-1/3$ and $4/3$, respectively.[31,32] Given that the integer steps experience twice the field intensity as half-integer steps, the field contribution at integer and half-integer values of t is proportional to $-2/3 + 4/3 = 2/3$ and $4/3$, respectively. At $t = 0$, it is proportional to $1/3$. These are the precise weightings used by the Simpson quadrature, and so we evaluate Eq. (8) using the Simpson method with a step size of $\Delta t = 1/2$. In practice, however, we only need to integrate up to $t = 10$ using the Simpson method, and then the rest of the integral can be performed analytically using $q_0(0,t) \approx (3\Delta^2/2\pi a^2 t)^{3/2}$.

For the next part of the calibration, we evaluate the disordered-state structure function for three polymerizations, $N = 16$, 32, and 64. In FTS, the structure function is given

This manuscript was accepted by J. Chem. Phys. Click here to see the version of record.

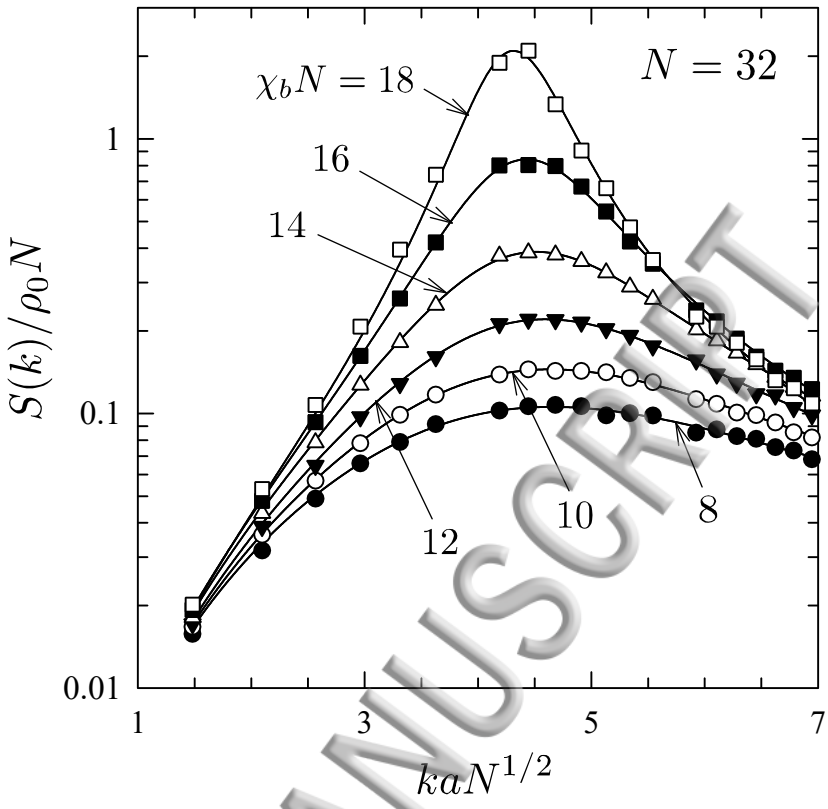

FIG. 2: Structure function, $S(k)$, for molecules of polymerization $N = 32$ calculated for different interaction parameters, χ_b. Symbols denote FTS results, and the curves are fits used to extract the peak height, $S(k^*)$.

by[24,27,33]

$$\frac{S(\mathbf{k})}{\rho_0 N} = \frac{n}{(V\chi_b)^2}\langle |W_-(\mathbf{k})|^2\rangle - \frac{1}{2\chi_b N} \ . \tag{9}$$

The size of the simulation box, $L = m\Delta$, is chosen such that the number of grid points ($m = 16 = 2^4$, $24 = 2^3 \times 3$, and $32 = 2^5$ used for $N = 16$, 32, and 64, respectively) only contains factors of 2 and 3. This aids the numerical efficiency of the fast Fourier transforms used in the pseudo-spectral algorithm.[32] Due to the finite size of the simulation box, the wavevector is only permitted to take on a discrete set of values: $\mathbf{k} = 2\pi(h, k, l)/L$, where h, k, and l are integers. Although the cubic box slightly breaks the isotropic symmetry, we average $S(\mathbf{k})$ over wavevectors of the same magnitude turning it into a function of $k \equiv |\mathbf{k}|$. Figure 2 plots $S(k)$ at a series of χ_b values for diblock copolymers of $N = 32$. The peaks, $S(k^*)$, are extracted from fits to the RPA structure function,[3] denoted by the solid curves in Fig. 2.

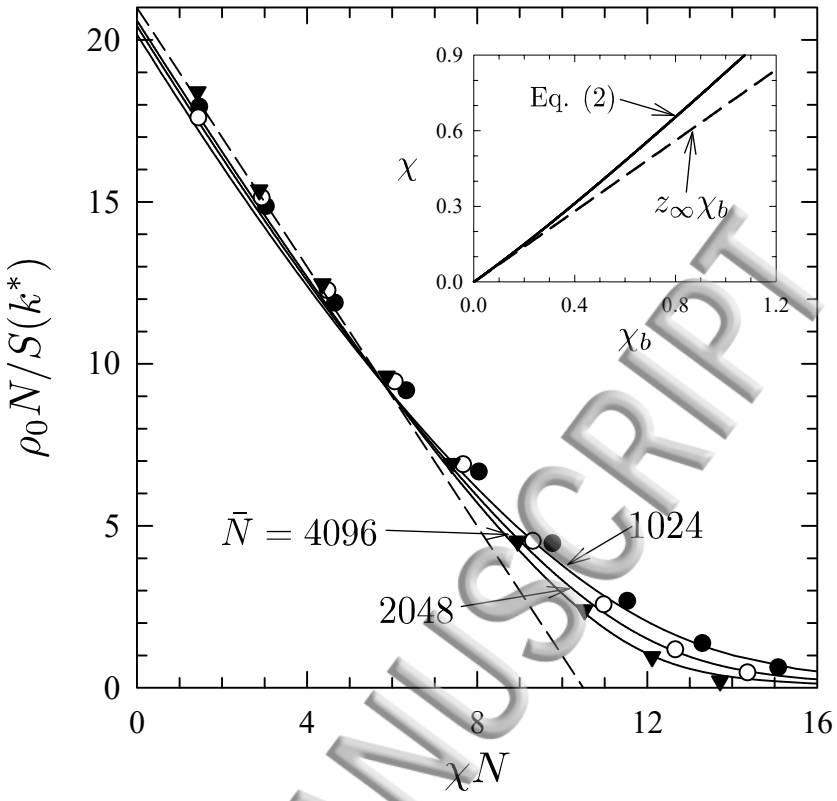

FIG. 3: Inverse peak height of the structure function, $S^{-1}(k^*)$, plotted in terms of the effective χ parameter for different invariant polymerization indexes, $\bar{N} = 64N$. Symbols denote FTS results, solid curves are ROL predictions, and the dashed line is the RPA prediction. The inset shows the nonlinear dependence of χ on χ_b, Eq. (2), with a solid curve and the linear approximation, $\chi \approx z_\infty \chi_b$, with a dashed line.

The final step of the calibration is to adjust the coefficients in Eq (2), c_1 and c_2, so as to match the peaks, $S(k^*)$, from the FTS to the predictions of ROL theory.[11,12] Figure 3 shows our best fit, where the FTS results are plotted with symbols and the ROL predictions are given by solid curves. The dashed line denotes the mean-field prediction from RPA.[3] The ROL predicts a slight deviation from RPA at small χN, which is well reproduced by particle-based simulations[7,13] but absent from our MC-FTS due to the saddle-point approximation. Therefore, our fit only includes the data points for $\chi N > 7$. The resulting coefficients are

$$c_1 = 0.916 \quad \text{and} \quad c_2 = 0.952 \ . \tag{10}$$

The inset of Fig. 3 shows the nonlinear relationship between χ and χ_b with a solid curve, while the dashed line denotes the linear approximation, $\chi \approx z_\infty \chi_b$.

IV. RESULTS

To test the calibration, we examine the order-disorder transition (ODT) of symmetric diblock copolymer melts for experimentally relevant values of $\bar{N} = 64N$. Past FTS[28,38] as well as particle-based simulations[39,40] have shown that two lamellar periods are sufficient to obtain reasonable estimates of the ODT. From previous experience,[27,28] the equilibrium period of the lamellar phase is accurately estimated by $D \approx 2\pi/k^*$, where k^* is the peak position of $S(k)$. Indeed, this was confirmed in our simulations of $S(k)$ by the period of the lamellar phase that spontaneous formed once χ_b exceeded the ODT. Our initial intention was to simulate polymers of $N = 16$, 32, and 64. Based on the estimated length of two periods, the appropriate sizes of the simulation box are $m = 12$, 17, and 24, respectively. However, the fast Fourier transform used by the pseudo-spectral algorithm would be particularly slow for $m = 17$, on account of it being a prime number.[27] Therefore, we choose to simulate $N = 28$ polymers, for which the appropriate box size is $m = 16$.

To locate the ODT, we simulate multiple replicas of the system at a series of χ_b values spanning the expected ODT, all initialized with disordered configurations. The replicas are run in parallel, each following the usual MC algorithm. The phase at each χ_b value is monitored by evaluating the order parameter $\langle\Psi\rangle$, which is an average of

$$\Psi = \left(\frac{N}{V}\right)^2 \max_{\mathbf{k}} |W_-(\mathbf{k})|^2 \ , \tag{11}$$

over the last 10^5 MCS. Past studies[27,28] have demonstrated that $\langle\Psi\rangle$ jumps from a small value in the disordered state to a large value in the lamellar phase.

During the simulation, highly metastable defects often nucleate impeding the formation of a well-ordered morphology, particularly when χ_b is large. To help remedy this problem, we implement parallel tempering,[41] whereby swaps between replicas at neighboring χ_b values are attempted every 10^3 MCS (see Ref. 27 for more details). In this way, defect structures are shifted to lower segregation, which allows them to anneal out more easily. As expected, all the ordered replicas exhibited two lamellar periods. Even with parallel tempering, the metastability of the disordered phase may cause an overestimation of $(\chi_b N)_{\mathrm{ODT}}$. Therefore, we run a second set of parallel tempering simulations starting from ordered lamellar configurations. This will generally result in an underestimation of $(\chi_b N)_{\mathrm{ODT}}$, thus allowing us to bracket the true equilibrium ODT.

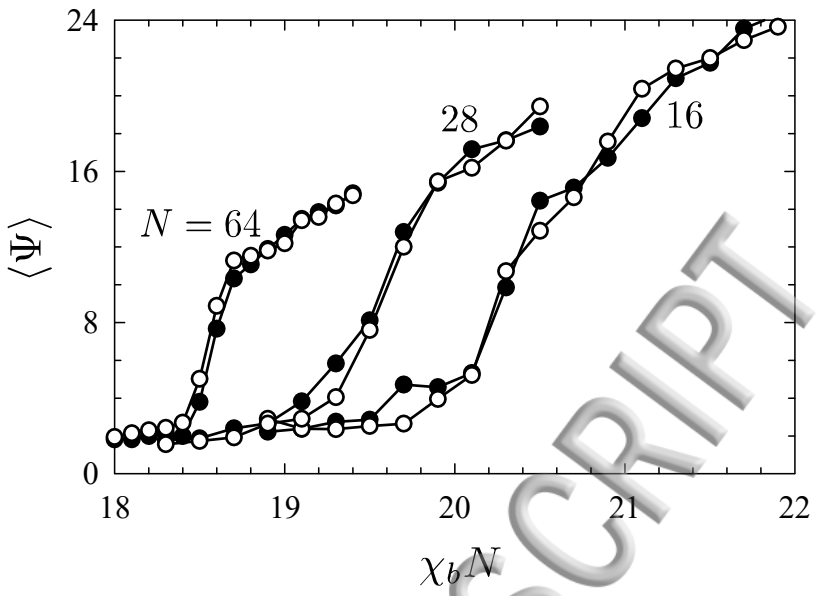

FIG. 4: Order parameter, $\langle\Psi\rangle$, from parallel-tempering simulations for molecules of polymerization $N = 16$, 28, and 64. Solid and open symbols denote simulations initialized with ordered and disordered configurations, respectively.

Figure 4 shows the order parameter resulting from pairs of runs for $N = 16$, 28, and 64. As it turns out, the runs from ordered and disordered configurations are nearly identical, indicating that non-equilibrium effects are negligible. However, the transitions are somewhat broadened due to the finite size of the simulation boxes, which makes it difficult to identify the ODT, particularly for $N = 16$.

To locate the transition for $N = 16$ more accurately, Fig. 5 plots histograms of Ψ for a series of χ_b values. Consistent with a first-order transition, there is a peak around $\Psi \approx 3$ that diminishes as χ_b increases, while a distinct peak near $\Psi \approx 20$ emerges. Visual inspection of configurations from the two peaks reveal disordered and lamellar configurations, respectively. The equilibrium ODT corresponds to the point where the two peaks are of comparable size, which in this case is $(\chi_b N)_{\rm ODT} \approx 20.4$. Similar histograms for $N = 28$ and 64 predict $(\chi_b N)_{\rm ODT} \approx 19.3$ and 18.5, respectively. These values do, indeed, correspond well with the sharp rises in $\langle\Psi\rangle$ observed in Fig. 4.

Figure 6 plots the above ODTs in terms of the effective χN and $\bar{N} = 64N$, and then compares them with the universal curve from Eq. (3). The main source of inaccuracy in our estimates of $(\chi N)_{\rm ODT}$ is undoubtedly from finite-size effects, which we cannot judge without performing simulations in larger simulation boxes. Nevertheless, the inaccuracy is probably

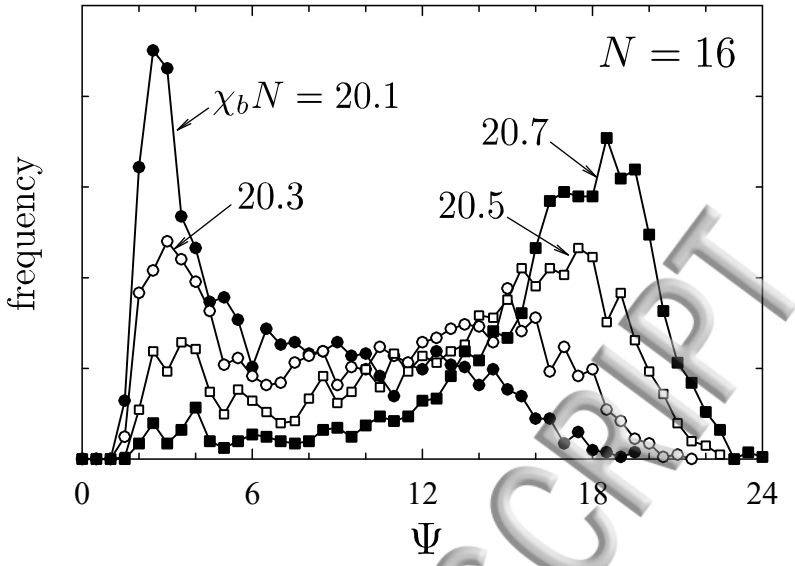

FIG. 5: Histograms of Ψ generated at different values of χ_b for diblock copolymers of polymerization $N = 16$.

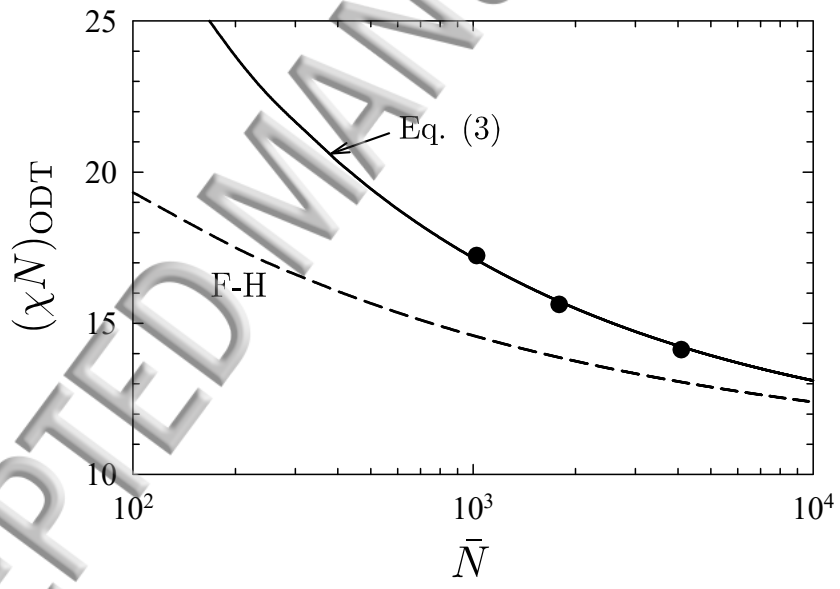

FIG. 6: Estimates of the ODT plotted in terms of the effective χ and the invariant polymerization index, $\bar{N}$. The solid curve denotes the universal prediction in Eq. (3),[13] and the dashed curve is the Fredrickson-Helfand prediction.[5]

at least as large as the symbols in Fig. 6, and thus our ODTs agree well with Eq. (3).

V. DISCUSSION

The UV divergence has been circumvented by treating the grid spacing, Δ, as a parameter in a discrete version of the GCM, and then mapping that model back onto the standard GCM using the Morse calibration. Because of the discrete grid, simulation results will depend somewhat on the numerical algorithm used to solve the diffusion equation, and therefore the algorithm is considered as part of the model. In our case, Eq. (6) is solved using the pseudo-spectral algorithm supplemented by Richard extrapolation,[31,32] with a contour step of $\Delta t = 1$. Furthermore, the Simpson quadrature used to evaluate the integral in Eq. (7) is also regarded as part of the model.

In particle-based simulations, the segment length, a, requires calibration as well. This is generally done by evaluating $R_0/N^{1/2}$ or $R_g/(6N)^{1/2}$ for neat homopolymer melts of polymerization N, and then extrapolating to the $N \to \infty$ limit.[9] The fact that MC-FTS reduce to mean-field theory for $\chi_b = 0$ implies that the a in Eq. (6) of the MC-FTS is, in fact, already the correct segment length. Hence, we conveniently avoid the need to calibrate the segment length.

Our particular calibration was performed for a grid spacing of $\Delta = a$ and a segment density of $\rho_0 = 8/a^3$, which gave $z_\infty = 0.7048$, $c_1 = 0.916$, and $c_2 = 0.952$ for the coefficients in Eq. (2). Naturally, a different choice of Δ/a and $a^3\rho_0$ would have resulted in different coefficients. In the case of z_∞, the dependence on these quantities is given by

$$z_\infty = 1 - \frac{p(\Delta/a)}{a^3\rho_0} \ , \tag{12}$$

where the function

$$p(\delta) = \frac{2}{\delta^3}\int_0^\infty q_0(0,t)dt \tag{13}$$

is evaluated by solving the diffusion equation for $q_0(\mathbf{r},t)$ with a grid spacing of $\Delta = \delta a$, which in fact can be done analytically as shown in the Appendix. As before, the integration is performed using the Simpson quadrature with a step size of $\Delta t = 1/2$. The resulting function, $p(\delta)$, is plotted in Fig. 7. Likewise, the other coefficients, c_1 and c_2, will depend on the same two quantities, but the determination of those dependencies would require computationally expensive simulations of $S(k)$. Therefore, we leave this for future consideration.

As shown in the Appendix and illustrated by the dashed line in Fig. 7, $p(\delta) \to 6\alpha/\pi\delta$ as $\delta \to \infty$, which implies that the linear approximation $\chi \approx z_\infty\chi_b$ is equivalent to the

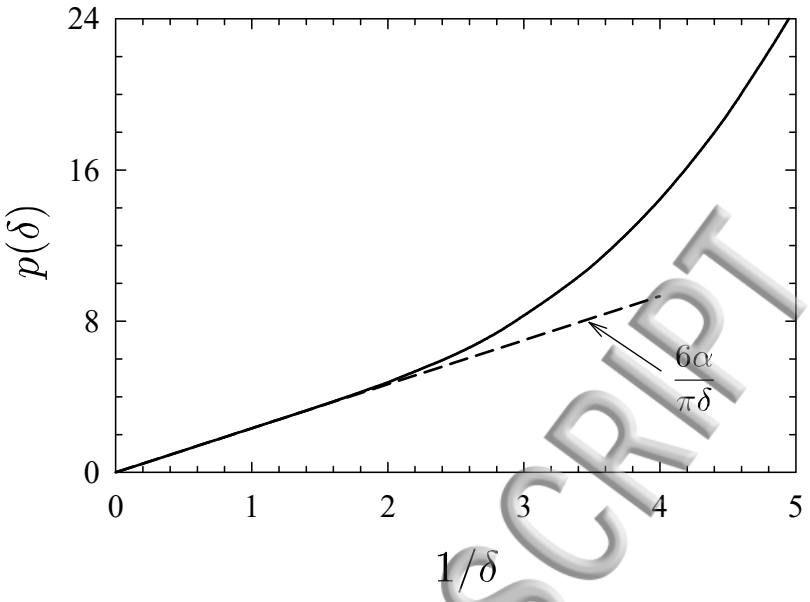

FIG. 7: The function controlling the Δ-dependence of z_∞ in Eq. (12). The dashed line denotes the asymptotic limit derived in the Appendix, which coincides with the renormalization in Eq. (1).

renormalization in Eq. (1), provided the FTS is performed on grids of $\Delta \gtrsim a$. In other words, the Morse calibration reduces to Eq. (1) for small χ_b, which implies that the two approaches for dealing with the UV divergence become equivalent at large $\bar{N}$. Similarly, the alternative renormalization proposed by Vorselaars and Matsen[28] is equivalent to $\chi = z(N)\chi_b$, where

$$z(N) = 1 - \frac{1}{\Delta^3 \rho_0 N} \int_0^N \int_0^N q_0(0, |t - t'|) dt' dt \tag{14}$$

is the fraction of intermolecular contacts among linear homopolymers of finite N. This is the same effective χ proposed by Müller and Binder,[8] and thus it has the same undesirable dependence on molecular weight and polymeric architecture.

The reason for the deviation between $\chi \approx z_\infty \chi_b$ and Eq. (1) at large δ, as implied by Fig. 7, is simple. If we neglect the Richardson extrapolation, the operator-splitting used by the pseudo-spectral algorithm[42] treats the polymers as a series of point-like beads connected by harmonic springs of unperturbed length a. Each of the beads experiences the field values corresponding to the spatial cell that they occupy. When $a \gg \Delta$, bonded beads are able to locate in distant cells thereby jumping past the intermediate cells, which violates the behavior of a continuous chain. On the other hand, a choice of $a \ll \Delta$ forces the polymer to have multiple beads in each of the cells that it visits, thus sampling the fields more than necessary. According to Fig. 7, our choice of $\Delta = a$ is somewhat conservative but not

regressively.

We intentionally chose $a^3\rho_0 = 8$ so that the polymerizations in our MC-FTS (i.e., $N = 16$ to 64) would correspond to experimentally relevant values of the invariant polymerization index (i.e, $\bar{N} \approx 1000$ to 4000). Given this choice, it would be impossible to consider significantly smaller values of $\bar{N}$, because the polymeric behavior would be lost if the number of segments, N, was too small. Although we could, in principle, simulate arbitrarily large $\bar{N}$ by increasing N, this would be computationally wasteful. The best way to access other intervals of $\bar{N}$ is to recalibrate χ for different values of $a^3\rho_0$.

The fixed grid spacing, Δ, generally prevents the lamellar phase from acquiring its ideal period. Although past studies[28,39,40] have shown that this has a relatively small effect on the predicted ODT, the period could perhaps be equilibrated by including the 'box' move from Ref. 28. This MC move involves a volume-conserving distortion of the simulation box, whereby the grid spacings in the x, y and z directions are changed to $\Delta_x = \lambda\Delta$, $\Delta_y = \lambda^{-1/2}\Delta$ and $\Delta_z = \lambda^{-1/2}\Delta$, respectively, while holding the number of grid points constant. Provided λ remains close to one, the renormalization in Eq. (1) is relatively unaffected. This will also be true of z_∞, given its equivalence to Eq. (1). If the same is true of $S(k)$, then the box move could be included without disrupting the Morse calibration. Nevertheless, this assumption needs to be tested before including the move.

Ideally, we would have simulated larger system sizes in order to assess the finite-size effects on the ODT. However, when we attempted simulations for three lamellar periods, the parallel tempering runs produced large metastability intervals preventing an accurate determination of the ODT. We also tried to locate the ODT using thermodynamic integration,[43] but this too resulted in large uncertainties due to statistical inaccuracies. The underlying problem is that the amplitudes of our MC moves decrease when applied to larger simulation boxes. This could very well be remedied by devising better MC moves. Another option is to perform standard Langevin simulations (L-FTS), with the same saddle-point approximation for $W_+(\mathbf{r})$.[33,34] We are currently exploring these possibilities, now that the issue of the UV divergence has been dealt with.

Naturally, the saddle-point approximation for $W_+(\mathbf{r})$ will result in some degree of inaccuracy. Although past studies[34,35] have shown the approximation to be accurate, this will become less so as $\bar{N}$ is reduced. The clearest evidence for this is the inability of MC-FTS to capture the departure of $S(k^*)$ from the RPA prediction at small χN, as seen in Fig. 3.

Nevertheless, this issue remains relatively minor for the level of fluctuations considered in this study.

CL-FTS avoid the saddle-point approximation, but they have their own challenges. In addition to the UV divergence, CL-FTS of the standard GCM experience an instability that prevents simulations at realistic values of $\bar{N}$.[25] However, the instability can be tamed by introducing compressibility. Delaney and Fredrickson[38] go further and smear all their interactions, so as to also remove the UV divergence. Naturally, a calibration is then required in order to map the resulting model back onto the standard (or canonical) GCM. In *lieu* of a methodology for the Morse calibration, they resorted to an *ad hoc* calibration of χ to match their ODT to Eq. (3).

The application of the Morse calibration to CL-FTS would be complicated by the fact that the athermal limit does not reduce to mean-field theory. Consequently, the evaluation of z_∞ would require simulations. Furthermore, the segment length would need to be calibrated, much in the same way it requires renormalization in ROL calculations.[11] Perhaps if $\bar{N}$ is not too small, it might be sufficient to use Eq. (8) for z_∞ and to ignore changes from the bare segment length. It would then just be a matter of repeating the fit in Fig. 3, using the $S(k^*)$ obtained from CL-FTS. It is not clear, however, whether CL-FTS would be able to, for example, capture the deviations of $S(k^*)$ from the RPA in Fig. 3. If too much smearing of the interactions is required, then the CL-FTS might not exhibit the universal behavior that we are ultimately interested in, until $\bar{N}$ is beyond the experimental regime.

VI. SUMMARY

Field-theoretic simulations (FTS) for the standard Gaussian-chain model (GCM) have been extended to experimentally relevant molecular weights. This was achieved using a new strategy for the UV divergence. Rather than trying to remove the divergence by renormalizing the interaction parameter, χ, according to Eq. (1), we simply fix the grid spacing, Δ, and the segment density, ρ_0, relative to the segment length, a. Due to the finite grid spacing, simulation results are sensitive to the choice of numerical methods and so they are treated as part of the model. In our case, this includes the pseudo-spectral algorithm with Richardson extrapolation used to solve the diffusion equation in Eq. (6) and the Simpson quadrature used to evaluate the integral in Eq. (7). Both algorithms use a step-size of $\Delta t = 1$, which

regulates N with the total number of steps along the polymer contour. The Morse calibration is then used to map our discrete version of the GCM back onto the continuous one.

The calibration relates the effective χ for the standard GCM to the bare χ_b used in the FTS by the functional form in Eq. (2), which involves three coefficients. The first coefficient, z_∞, represents the fraction of intermolecular contacts among infinitely long polymers in an athermal melt (i.e., $\chi_b = 0$) and is obtained by solving the diffusion equation for zero field. The remaining two coefficients, c_1 and c_2, are determined by fitting the peak of the structure function, $S(k^*)$, for disordered melts of symmetric diblock copolymer to predictions from renormalized one-loop (ROL) theory.[11,12] Our particular calibration was performed for $\Delta/a = 1$, which provides a good balance between the spatial and contour steps of the diffusion equation, and $a^3\rho_0 = 8$, which is ideal for simulating diblock copolymers of $10^3 \lesssim \bar{N} \lesssim 10^4$. The resulting coefficients of the calibration are $z_\infty = 0.7048$, $c_1 = 0.916$, and $c_2 = 0.952$.

To facilitate standard Monte Carlo simulations (MC-FTS), the incompressibility condition was only satisfied in the mean-field approximation. This has the added benefit of simplifying the calculation of z_∞ and foregoes the need to calibrate the segment length. However, it did result in some inaccuracy. In particular, it prevented us from matching $S(k^*)$ to ROL theory at small χN (see Fig. 3). For the range of $\bar{N}$ considered in this study, the resulting inaccuracy appears to be small.

Indeed, Fig. 6 shows that the calibration brings the order-disorder transition (ODT) from MC-FTS into agreement with the universal prediction, Eq. (3), from particle-based simulations.[13] Although the calibration was performed for symmetric diblock copolymers, the resulting χ is applicable to all architectures. Thus, MC-FTS can now be readily applied to any AB-type block copolymer system. For those researchers already implementing SCFT using the pseudo-spectral algorithm, the switch to MC-FTS will be particularly straightforward.

Acknowledgments

We thank Russell Spencer for useful discussions. This work was supported by NSERC of Canada and computer resources were provided by SHARCNET of Compute Canada.

Appendix

Here, we derive the analytical approximation for, $p(\delta)$, at large δ, plotted in Fig. 7 with a dashed line. In the absence of fields, the pseudo-spectral algorithm becomes a true spectral algorithm, and therefore it follows that

$$q_0(\mathbf{r},t) = \frac{1}{m^3}\sum_{\mathbf{k}} e^{i\mathbf{k}\cdot\mathbf{r}-a^2k^2t/6} \ . \tag{15}$$

Evaluating this at the origin, we obtain

$$q_0(0,t) = \left[\frac{1}{m}\sum_{k_x} e^{-a^2k_x^2t/6}\right]^3 , \tag{16}$$

where we have used the fact that the sums over k_y and k_z are equivalent to the one over k_x. The remaining sum is over the wavenumbers $k_x = 2\pi n/m\Delta$, where n takes on integer values from $-m/2$ to $m/2$. In the thermodynamic limit, m approaches infinity, which allows the sum to be converted to an integral giving

$$q_0(0,t) = \left[\frac{1}{2\xi}\int_{-\xi}^{\xi} e^{-u^2}du\right]^3 = \left[\frac{\sqrt{\pi}}{2\xi}\mathrm{erf}(\xi)\right]^3 , \tag{17}$$

where the integration variable is $u = ak_x\sqrt{t/6}$ and

$$\xi = \frac{\pi}{\delta}\sqrt{\frac{t}{6}} \ . \tag{18}$$

As explained previously, the integral of $q_0(0,t)$ in Eq. (13) for $p(\delta)$ should, in principle, be performed using the Simpson quadrature with $\Delta t = 1/2$. However, if δ is large, then $q_0(0,t)$ becomes a slowly varying function over the entire range of t, and thus the Simpson method is well approximated by the analytical calculation of the integral. Transforming the integration variable from t to ξ then leads immediately to

$$p(\delta) \approx \frac{3}{\delta\sqrt{\pi}}\int_0^{\infty}\frac{\mathrm{erf}^3(\xi)}{\xi^2}d\xi = \frac{2.332654}{\delta} \ . \tag{19}$$

Equating this to $6\alpha/\pi\delta$ gives $\alpha = 1.221375$, which is the same value calculated previously in Ref. 27, albeit with a couple more significant digits.

* Electronic address: mwmatsen@uwaterloo.ca

[1] M. W. Matsen, J. Phys.: Condens. Matter **14**, R21 (2002).

[2] E. Helfand, J. Chem. Phys **63**, 999 (1975).

[3] L. Leibler, Macromolecules **13**, 1602 (1980).

[4] A. N. Semenov, Sov. Phys. JETP **61** 733 (1985).

[5] G. H. Fredrickson and E. Helfand, J. Chem. Phys. **87**, 697 (1987).

[6] M. W. Matsen and F. S. Bates, Macromolecules **29**, 1091 (1996).

[7] J. Glaser, J. Qin, P. Medapuram, M. Müller, and D. C. Morse, Soft Matter **8**, 11310 (2012).

[8] M. Müller and K. Binder, Macromolecules **28**, 1825 (1995).

[9] J. Qin and D. C. Morse, J. Chem. Phys. **130**, 224902 (2009).

[10] J. Glaser, P. Medapuram, and D. C. Morse, Macromolecules **47**, 851 (2014).

[11] P. Grzywacz, J. Qin, and D. C. Morse, Phys. Rev. E **76**, 061802 (2007).

[12] J. Qin, P. Grzywacs, and D. C. Morse, J. Chem. Phys. **135**, 084902 (2011).

[13] J. Glaser, P. Medapuram, T. M. Beardsley, M. W. Matsen, and D. C. Morse, Phys. Rev. Lett. **113**, 068302 (2014).

[14] P. Medapuram, J. Glaser, and D. C. Morse, Macromolecules **48**, 819 (2015).

[15] T. M. Beardsley and M. W. Matsen, Phys. Rev. Lett. **117**, 217801 (2016).

[16] T. Ghasimakbar and D. C. Morse, Macromolecules **51**, 2335 (2018).

[17] V. Ganesan and G. H. Fredrickson, Europhys. Lett. **35**, 16 (2001).

[18] G. H. Fredrickson, V. Ganesan and F. Drolet, Macromolecules **35**, 16 (2002).

[19] G. H. Fredrickson, *The Equilibrium Theory of Inhomogeneous Polymers* (Oxford University Press, New York, 2006).

[20] G. H. Fredrickson, Soft Matter **3**, 1329 (2007).

[21] Y. X. Liu, K. T. Delaney and G. H. Fredrickson, Macromolecules **50**, 6263 (2017)

[22] R. K. W. Spencer and M. W. Matsen, J. Chem. Phys. **148**, 204907 (2018).

[23] R. K. W. Spencer and M. W. Matsen, J. Chem. Phys. **149**, 184901 (2018).

[24] M. Müller and F. Schmid, in *Advanced Computer Simulation Approaches for Soft Matter Sciences II* edited by C. Holm and K. Binder (Springer-Verlag, Berlin, 2005).

[25] J. Koski, H. Chao, and R. A. Riggleman, J. Chem. Phys. **139**, 244911 (2013).

[26] M. O. de la Cruz, S. F. Edwards, I. C. Sanchez, J. Chem. Phys. **89**, 1704 (1988).

[27] P. Stasiak and M. W. Matsen, Macromolecules **46**, 8037 (2013).

[28] B. Vorselaars, P. Stasiak, and M. W. Matsen, Macromolecules **46**, 9071 (2015).

[29] R. K. W. Spencer and M. W. Matsen, Macromolecules **49**, 6116 (2016).

[30] R. K. W. Spencer and M. W. Matsen, Macromolecules **51**, 4747 (2018).

[31] A. Ranjan, J. Qin, and D. C. Morse, Macromolecules **41**, 942 (2008).

[32] P. Stasiak and M. W. Matsen, Eur. Phys. J. E **34**, 110 (2011).

[33] E. Reister, M. Müller, and K. Binder, Phys. Rev. **64**, 041804 (2001).

[34] A. Alexander-Katz and G. H. Fredrickson, Macromolecules **40**, 4075 (2007).

[35] D. Düchs, V. Ganesan, G. H. Fredrickson, and F. Schmid, Macromolecules **36**, 9237 (2003).

[36] D. Düchs and F. Schmid, J. Chem. Phys. **121**, 2798 (2004).

[37] In the absence of fields, the separation, $\mathbf{r}$, between the $s = 0$ and $s = t$ monomers is unaffected by the tails of the chain (i.e., $s < 0$ and $s > t$), and therefore its distribution is just given by the propagator of the intervening chain (i.e., $0 \leq s \leq t$).

[38] K. T. Delaney and G. H. Fredrickson, J. Phys. Chem. B **120**, 7615 (2016).

[39] T. M. Beardsley and M. W. Matsen, Eur. Phys. J. E **32**, 255 (2010).

[40] A. Arora, D. C. Morse, F. S. Bates, and K. D. Dorfman, Soft Matter **11**, 4862 (2015).

[41] D. J. Earl and M. W. Deem, Phys. Chem. Chem. Phys. **7**, 3910 (2005).

[42] K. O. Rasmussen and G. Kalosakas, J. Polym. Sci., Part B **40**, 1777 (2002).

[43] R. K. W. Spencer, B. Vorselaars, and M. W. Matsen, Macromol. Theory Simul. **26**, 1700036 (2017).

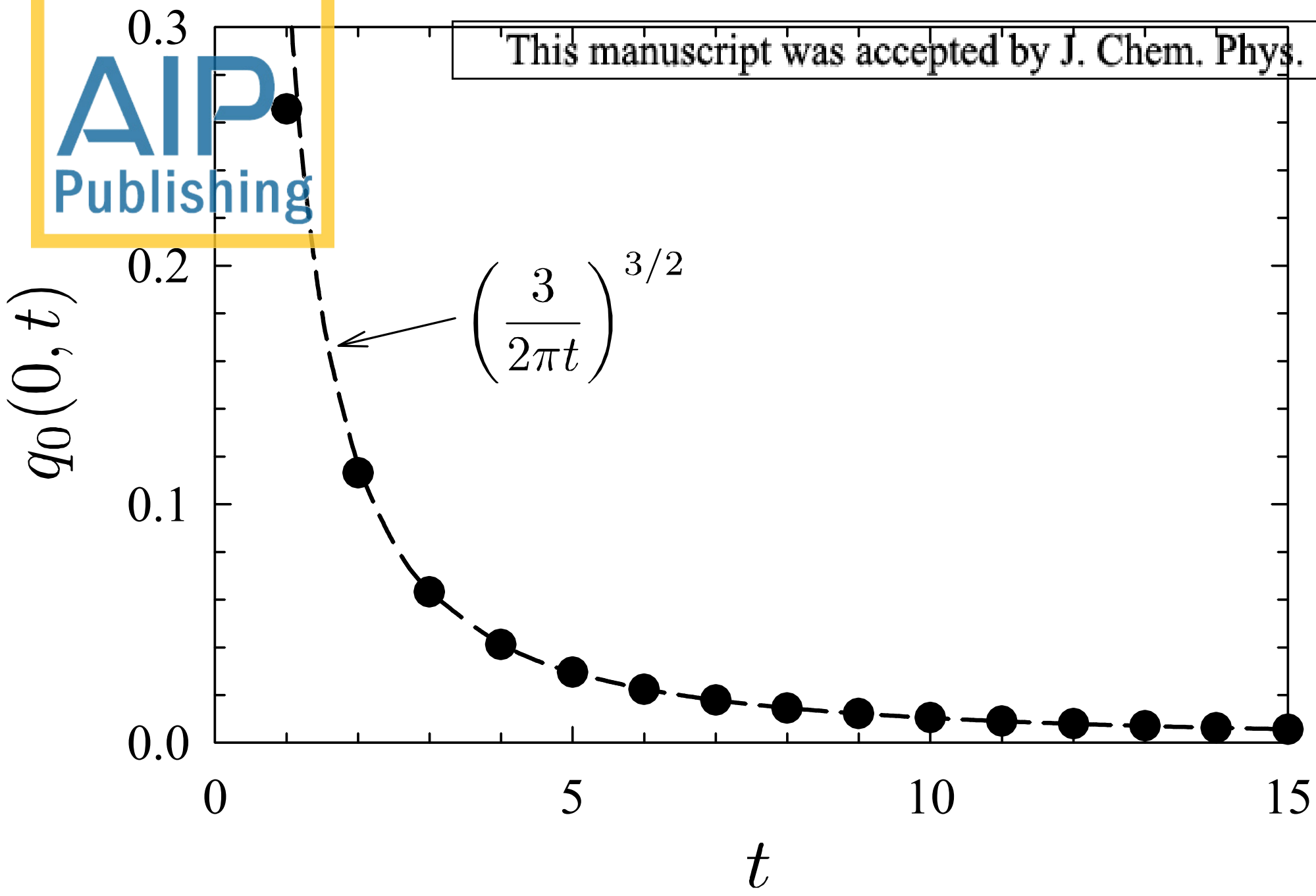

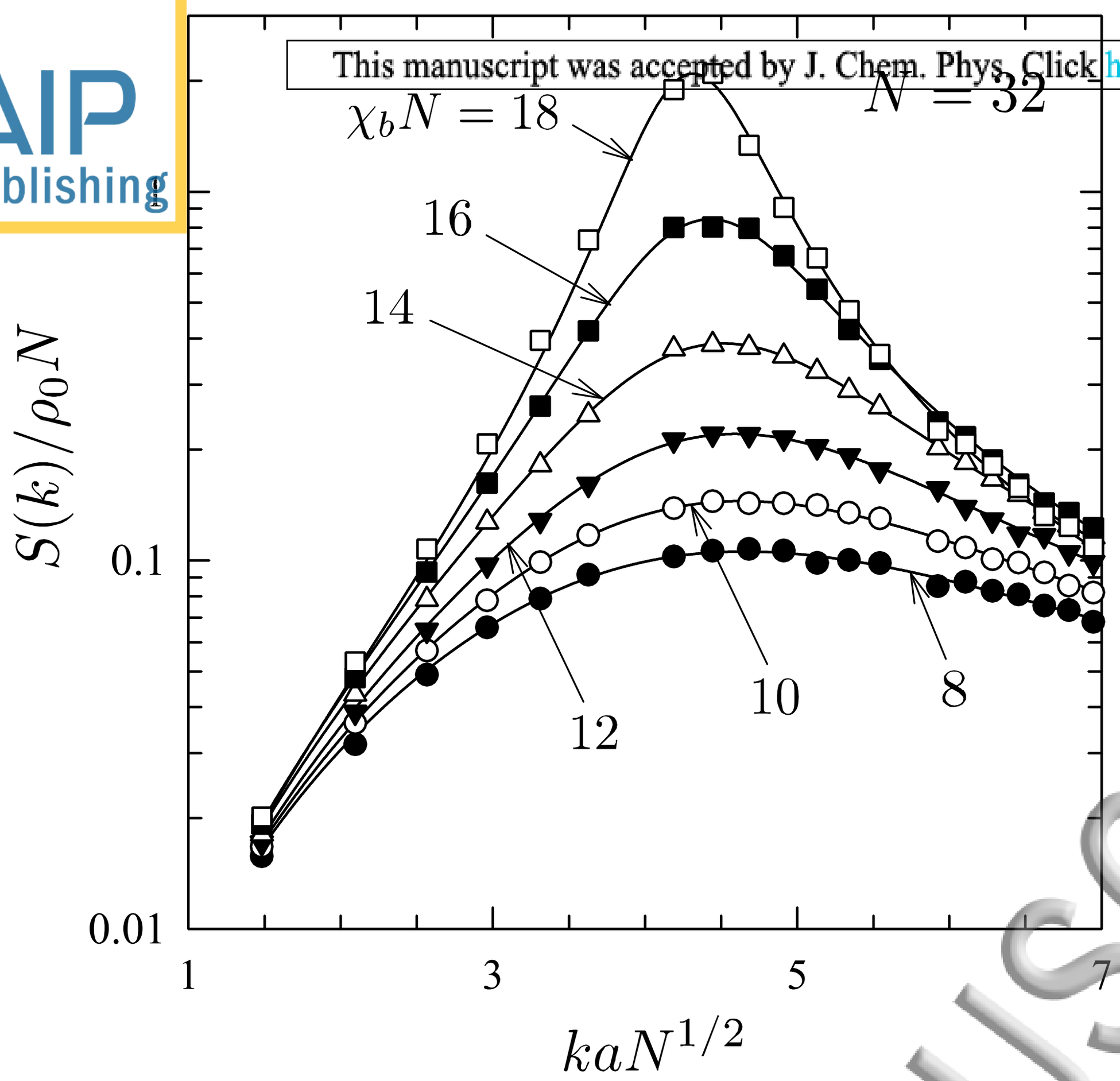

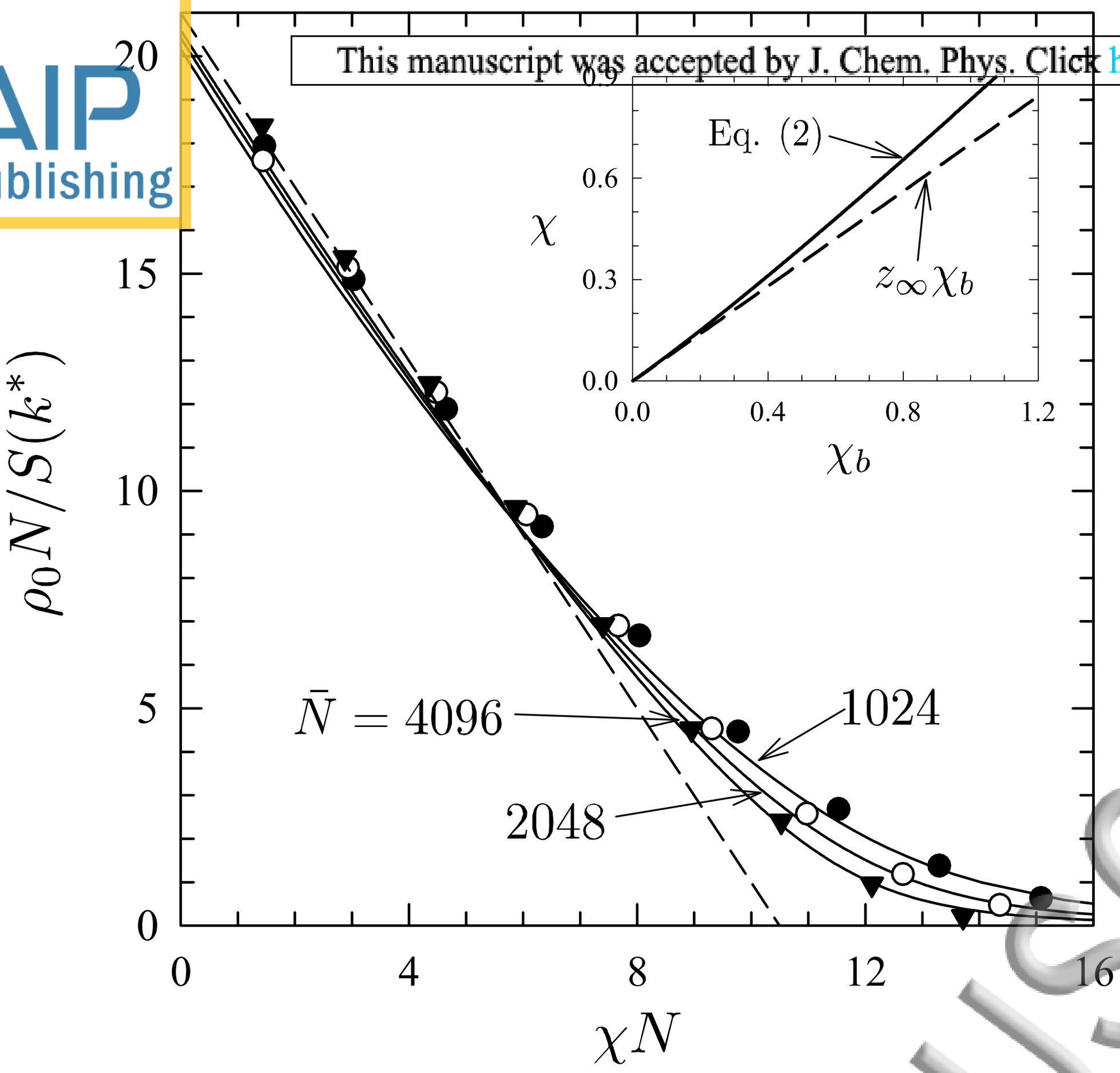

This manuscript was accepted by J. Chem. Phys.